Nanorod alignment

Effect of the Orientation of CdSe Nanorods on the Electron Mobility of CdSe/P4VP Nanodomains Self-Assembled within a Poly(styrene-b-4-vinylpyridine) Diblock Copolymer Thin Film**

*Chung-Ping Li, Siao-Wei Yeh, Han-Chang Chang, Jung Y. Huang, and Kung-Hwa Wei**

Block copolymers are versatile platform materials because they can self-assemble—if they have appropriate compositions and are subjected to suitable conditions—into various nanostructures having period thicknesses between 10 and 100 nm through microphase separation of incompatible blocks.[1,2] Nanostructured block copolymers can be used as templates for selectively controlling the spatial position of semiconductor nanoparticles within one of the blocks.[3–5] For example, the selective sequestrations of pre-synthesized CdS,[6a,e–f] CdSe,[3c] and TiO2[6b] nanoparticles into one block of a diblock copolymer can be performed by ensuring the presence of strong interactions between that block and the surface ligands of the nanoparticles. Block copolymers can also be used as nanoreactors for the synthesis of nanomaterials. For example, quasi-regular arrays of Au clusters[5a] and TiO2 needles[6c] have been obtained through the selective sequestration of metal ions into one block of poly(styrene-b-vinylpyridine).

The unique optical and electrical properties of one-dimensional (1D) semiconductor nanostructures, such as nanorods (NRs) and nanowires (NWs), can be exploited for use in a number of applications, including solar cells, photonic crystals, lasers, transistors, and sensors.[7,8,11a,b] To take full advantage of the material properties of these 1D nanostructures, they must be pre-aligned or ordered in some other way. Several physical and chemical strategies have been used for the alignment or ordering of arrays of 1D nanostructures. Examples for in-plane two-dimensional (2D) arrays include the unidirectional alignment of CdSe NRs,[9] the assembly of BaCrO4 NR monolayers through the use of the Langmuir–Blodgett technique,[10] and the alignment of a liquid-crystalline phase of CdSe NRs through surface deposition.[11c] For out-of-plane 2D arrays, some examples are the use of electron-beam (e-beam) lithography to obtain arrays of CdSe pillars and TiO2 nanoneedles through electrochemical deposition and solution crystal growth[12,6d] and the preparation of a periodic array of uniform ZnO NWs through vapor-phase transport and catalytic growth.[13] Although there are many bottom–up growth techniques for preparing 1D nanostructures in the out-of-plane 2D arrays and many techniques for pre-synthesized NRs in the in-plane 2D arrays, finding techniques for arranging pre-synthesized NRs in out-of-plane 2D arrays remains a great challenge.

The powerful aligning force of an electric field can be used to manipulate the orientation of anisotropic materials by taking advantage of their different anisotropic dielectric constants. Examples of this approach include the alignment of ZnO NRs and Au NWs,[14] the alignment of carbon nanotubes suspended in a columnar liquid-crystalline polymer melt,[15] and the electrically induced sphere-to-cylinder transition and patterning in diblock copolymer films.[16] In this present study, we applied an electric field to induce the orientation of CdSe NRs that had been self-assembled in the poly(4-vinylpyridine) (P4VP) nanodomains of a poly(styrene-b-4-vinylpyridine) (PS-b-P4VP) diblock copolymer thin film. We varied the number of CdSe nanorods incorporated in the P4VP nanodomains by controlling the strength of the polar interactions and the loading concentration. The electron mobilities and the electron-barrier heights of the CdSe/P4VP nanodomains incorporating out-of-plane and in-plane CdSe NRs were monitored.

Scheme 1 illustrates the process we used to prepare a monolayered (CdSe/P4VP)-b-PS thin film. Pyridine-modified CdSe NRs and the PS-b-P4VP block copolymer were dissolved and mixed in pyridine; the CdSe NRs were distributed selectively in the P4VP phase as a result of their preference for experiencing polar interactions. Subsequently, toluene, which is a good solvent for PS but a poor one for P4VP, was added to form a solution containing micelles having CdSe/P4VP cores and PS shells. Figure 1 displays TEM images of the P4VP domains of PS-b-P4VP samples containing different amounts of CdSe NRs. The dark regions represent the CdSe NRs (because of the high electron density of cadmium). The orientation of these CdSe NRs was largely in the plane direction of the PS-b-P4VP film. The interdomain distance of CdSe/P4VP domains was about 90 nm. In Figure 1a and b, where the loading concentrations of CdSe NRs were 65 and 48%, respectively, the average numbers of NRs incorporated within single P4VP nanodomains were approximately five and three, respectively. When the loading amount was 33%, some individually distinct CdSe nanorods were incorporated into the P4VP nanodomains (Figure 1c).

[*] C. P. Li, H. C. Chang, Prof. K. H. Wei
Department of Materials Science and Engineering
National Chiao Tung University
1001 Ta Hsueh Road, Hsinch 30050 Taiwan (ROC)
Fax: (+886)35-724727
E-mail: khwei@mail.nctu.edu.tw

Dr. S. W. Yeh
Center for Nano Science and Technology
National Chiao Tung University
1001 Ta Hsueh Road, Hsinch 30050 Taiwan (ROC)

Prof. J. Y. Huang
Department of Electro-Optical Engineering
National Chiao Tung University
1001 Ta Hsueh Road, Hsinch 30050 Taiwan (ROC)

Supporting information for this article is available on the WWW under http://www.small-journal.com or from the author.

WILEY InterScience® DISCOVER SOMETHING GREAT
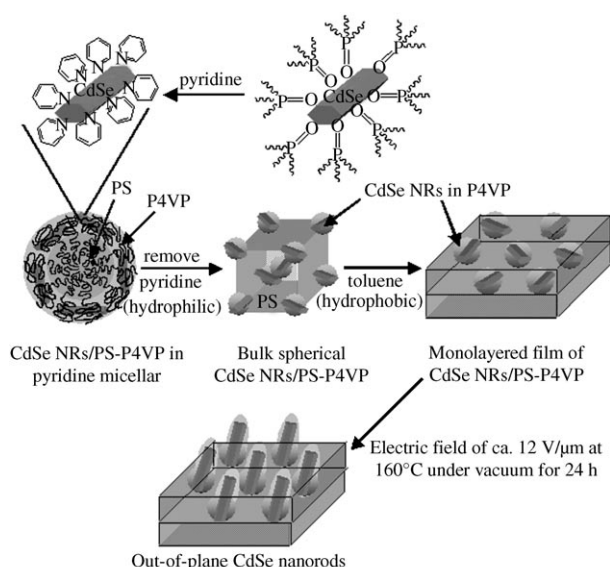
Scheme 1. Fabrication of a self-assembled (CdSe/P4VP)-*b*-PS thin film through the selective incorporation of dispersed pre-synthesized CdSe NRs into P4VP domains.

Figure 2a displays an SEM image of the tilted substrate of an as-prepared 33% (CdSe/P4VP)-*b*-PS thin film. Some small islands (diameters: circa 30 nm), which represent the CdSe/P4VP domains, appear because the CdSe NRs were not totally horizontally aligned with respect to the substrate and because their lengths (50 nm) were slightly larger than the size of the P4VP domain. Figure 2b presents an SEM image of the tilted substrate of a 33% (CdSe/P4VP)-*b*-PS thin film after it had experienced an applied electric field of 12 V μm^{-1} at 160°C under vacuum for 24 h. The protruding CdSe NRs appear to be oriented by about 65° with respect to the plane of the P4VP-*b*-PS thin film. The applied electric field induced charge separation, and the resulting polarization generated a net dipole moment, which aligned the long axes of the CdSe NRs parallel to the applied electric field. The force on the NRs in an electric field is expressed to a good first approximation by Equation (1):[17]

$$f = \vec{P} \cdot \partial \vec{E} / \partial r = (\varepsilon - 1) \cdot \partial \left(\left| \vec{E} \right|^2 \right) / 8\pi \partial r \qquad (1)$$

where f is the force per unit volume, $\vec{P}$ is the polarization, $\vec{E}$ is the electric field strength, r is the NR radius, and ε is the dielectric constant. Because the dielectric constant of the long axis ($\varepsilon_{\parallel} = 10.2$) of a CdSe NR is larger than that of the short axis ($\varepsilon_{\perp} = 9.33$),[18] the induced force along the long axis is larger than that along the short axis; thus, the long axis of the CdSe NR tends to align parallel to the applied electric field more so than does its short axis. The orientations (equilibrium angles) of the CdSe NRs appear to be determined by both the induced polarization force on the NRs and the viscous force of the P4VP domain surrounding them. The critical field strength, where the alignment can be turned on and off, is 12 V μm^{-1} (Figure S1 of the Sup-
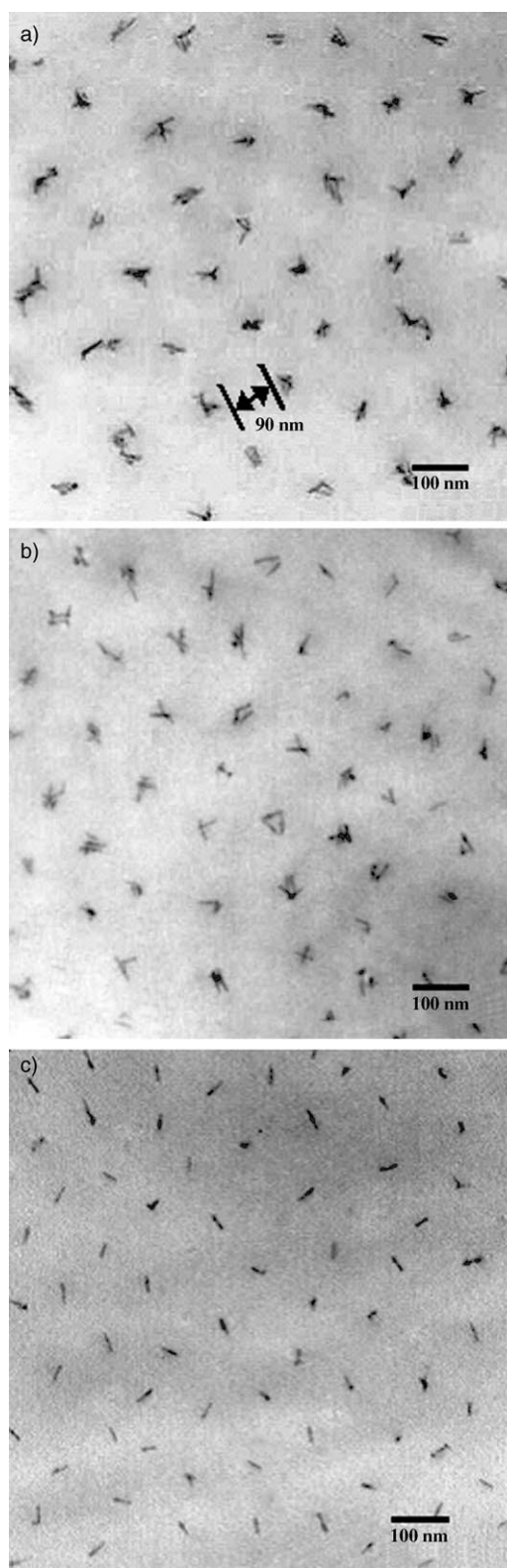

Figure 1. TEM images, obtained without staining, of thin films of a) 65%, b) 48%, and c) 33% (CdSe/P4VP)-*b*-PS.

porting Information). The states of the (CdSe/P4VP)-*b*-PS thin films before and after applying the electric field is shown in Scheme 1.
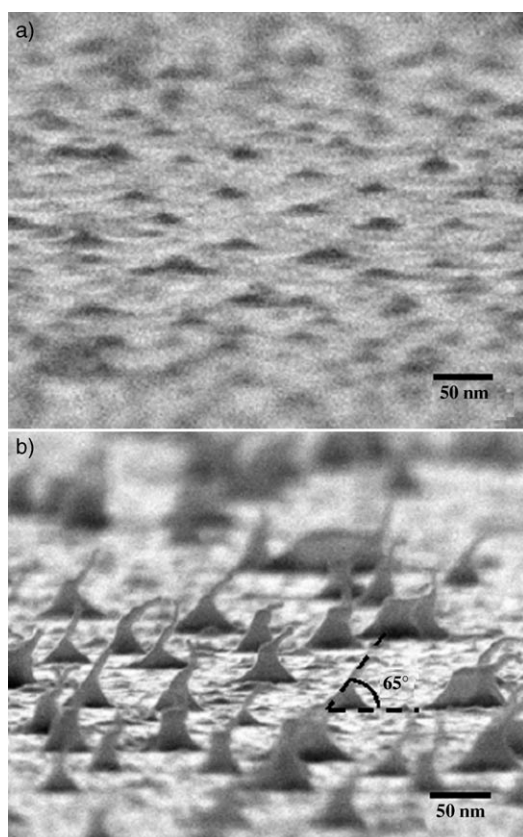
Figure 2. SEM images of 33% (CdSe/P4VP)-*b*-PS thin films prepared a) in the absence and b) in the presence of an applied electric field.

Figure 3a displays a cross-sectional TEM image of a 33% (CdSe/P4VP)-*b*-PS thin film that has not been subjected to an applied electric field. The dark regions at the top and bottom of this image are the Al and Pt electrodes; the lighter region is the domain of the CdSe/P4VP composite. The dark rods are the CdSe NRs, which are aligned horizontally with respect to the electrodes. Because the CdSe NRs are not aligned completely parallel to the *x* axis, their observed lengths are not their true lengths. The distance from the side surface of the CdSe NR to the surface of the Al electrode and to the Pt electrode is about 13 nm. Figure 3b displays a cross-sectional TEM image of a 33% (CdSe/P4VP)-*b*-PS thin film that has been subjected to an applied electric field. A micellar solution of 33% (CdSe/P4VP)-*b*-PS in toluene was spin-coated at 5000 rpm for 60 s on Pt-coated Kapton; an aluminized Kapton film comprised the top electrode for the applied electric field. After applying the electric field, the aluminized Kapton film was removed and a layer of Al (200 nm) was vacuum-deposited as the top electrode. The sandwiched sample was placed into an epoxy capsule, which was cured at 70 °C for 48 h in a vacuum oven. The cured epoxy samples were microtomed using a Leica Ultracut Uct into approximately 90-nm-thick slices. In the image, the dark bars are the CdSe NRs; their angle of orientation is about 65°. These NRs are about 50 nm long and 5 nm wide. The distance between the Al electrode and the CdSe NR is about 8 nm; the CdSe NR is much closer to the Pt electrode. The insets of Figure 3a and 3b present the
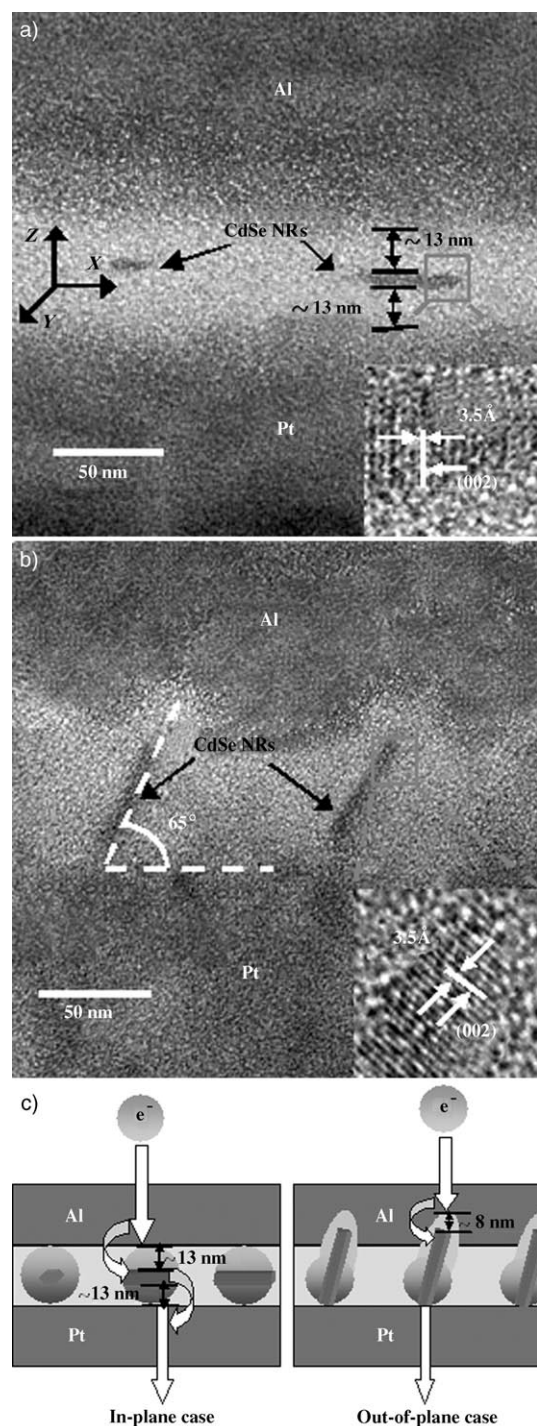

Figure 3. Cross-sectional TEM images of 33% (CdSe/P4VP)-*b*-PS thin films prepared a) in the absence of and b) in the presence of an applied electric field. The insets display the respective HRTEM lattice images of a CdSe NR incorporated within a single P4VP nanodomain of (CdSe/P4VP)-*b*-PS. c) A schematic depiction of the electron transport process.

high-resolution TEM (HRTEM) lattice images of CdSe NRs incorporated within single nanodomains of (CdSe/P4VP)-*b*-PS in the absence and presence of the electric field, respectively. The orientation of these wurtzite CdSe

NRs is along the [00l] direction, with a spacing between adjacent (002) lattice planes of approximately 3.5 Å.

Figure 4 displays the averaged current-density–electric-field (J–E) curves of a single CdSe/P4VP nanodomain in a PS matrix incorporating various amounts of out-of-plane
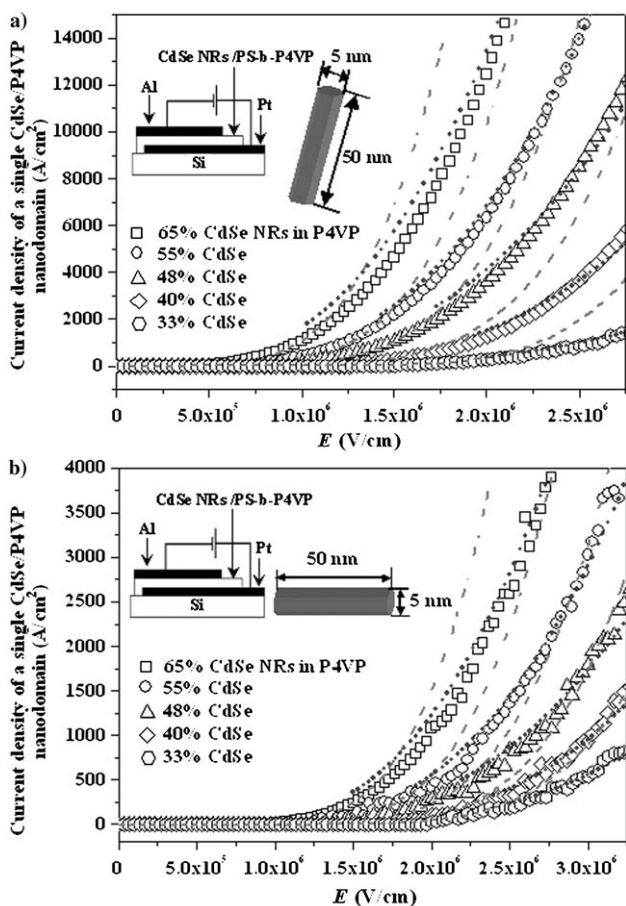
and in-plane CdSe NRs. These plots were obtained and derived from measurements of a device sandwiched between a Pt-coated Si wafer (bottom electrode) and an Al film (top electrode). We assume that the current flows through the CdSe/P4VP nanodomain, because of the much higher resistance of the PS phase. The current density of a single nanodomain can, therefore, be calculated from the density of the CdSe/P4VP nanodomain in the PS phase by using the following parameters obtained from the TEM image:

the area of the Al electrode was 1.96×10^{-3} cm^2 and the density of the CdSe/P4VP nanodomain in the PS phase was 3.1×10^9 cm^{-2}. The number of CdSe/P4VP nanodomains under the Al electrode, i.e., the product of the area of the Al electrode and the density of CdSe/P4VP nanodomains, is approximately 6×10^6. The value of J is obtained by dividing the current first by the number of CdSe/P4VP nanodomains and then by its area. The zero-current regions arise from electron tunneling from the Al electrode through the P4VP surrounding the CdSe NRs and to the conduction band of the CdSe NRs, which must overcome the electron-barrier height (ϕ_e) of the P4VP between the electrode and CdSe. A tunneling process can be modeled accurately using the Fowler–Nordheim (FN) equation, which can be expressed as Equation (2):[19]

$$J(E) = \frac{A_{\mathrm{eff}} q^3 E^2 m}{8\pi\, h \phi_e m^*} \exp\left[\frac{-8\pi\sqrt{2m^*}\,\phi_e^{3/2}}{3h\,q\,E} \right] \qquad (2)$$

where A_{eff} is the effective contact area, E is the applied electric field, and q, m^*, m, and h are the electron's charge and effective mass, free electron mass, and Planck's constant, respectively. By fitting the zero-current regions of the J–E curves to the FN theory, we obtained the values of ϕ_e that are presented in Table 1. The electron-barrier height from the electrode to the nanodomain decreased monotonically when the amount of CdSe increased in both the out-of-plane and in-plane cases, owing to the fact that the distance between the Al electrode and CdSe NRs decreased at higher densities of CdSe NRs. The electron-barrier heights in the out-of-plane cases were lower than those in the in-plane cases because the distance between the Al electrode and the CdSe NR was smaller in the out-of-plane case (Figure 3c). With regard to the electron mobility in the higher-electric-field region, the J–E curve can be described using a space-charge-limited current (SCLC) model, which can be expressed as Equation (3):[20]

$$J = \frac{9}{8}\varepsilon\varepsilon_0 \mu(E)\frac{E^2}{L} = \frac{9}{8}\varepsilon\varepsilon_0 \mu_0 \exp(\sqrt{E/E_0})\frac{E^2}{L} \qquad (3)$$

where ε is the dielectric constant of the nanorod/P4VP nanodomain, ε_0 is the vacuum permittivity, μ is the field-dependent electron mobility, L is the thickness of the thin film, μ_0 is the zero-field mobility, and E_0 is the field coefficient. By fitting the higher-electric-field regions of the J–E curves to this SCLC model, we obtained the values of μ_0

Figure 4. Averaged current-density–electric-field (J–E) curves of a single CdSe/P4VP nanodomain in a PS matrix incorporating various contents of a) out-of-plane and b) in-plane CdSe NRs. The dashed lines denote best fits to the FN equation; the dotted lines denote best fits to the SCLC model, which includes the field-dependent mobility.

Table 1. Electron-barrier heights (ϕ_e), electron mobilities (μ_0), and field coefficients (E_0) for in-plane and out-of-plane CdSe NRs incorporated within P4VP nanodomains in a PS matrix.

vol% of CdSe in P4VP	In-plane			Out-of-plane		
	$\phi_e \times$ (m/m*)$^{-1/3}$ [eV]	$\mu_0 \times 10^4$ [cm^{2}V^{-1}s^{-1}]	$E_0 \times 10^{-4}$ [Vcm^{-1}]	$\phi_e \times$ (m/m*)$^{-1/3}$ [eV]	$\mu_0 \times 10^4$ [cm^{2}V^{-1}s^{-1}]	$E_0 \times 10^{-4}$ [Vcm^{-1}]
33	1.66	1.2	5.8	1.45	9.3	6.2
40	1.54	4.1	5.6	1.35	32.3	5.8
48	1.43	17.6	6.1	1.21	141.5	5.6
55	1.37	31.1	5.9	1.16	248.4	6.3
65	1.29	90.2	5.7	1.05	723.2	5.9

and E_0 presented in Table 1. For both the out-of-plane and in-plane cases, the electron mobility increased monotonically when the amount of CdSe increased because the distance between the CdSe NRs decreased at higher nanorod densities. The electron mobilities in the out-of-plane cases were about eight times larger than those of the in-plane cases because the CdSe NRs were much closer to the Pt electrode in the former system (Figure 3c). Because the value of E_0 is material-dependent, these two cases provide similar values.

In conclusion, we have aligned CdSe nanorods, which were self-assembled in the P4VP nanodomains of a PS-*b*-P4VP diblock copolymer thin film, through the use of polarization forces created by an applied electric field. The electron mobilities of the CdSe/P4VP nanodomains in the out-of-plane cases were about eight times larger than those in the in-plane cases. In both the out-of-plane and in-plane cases, the electron mobility increased upon increasing the number of CdSe nanorods. The height of the electron barrier from the Al electrode to the nanodomain in the out-of-plane case was much smaller than that in the in-plane case; in both the out-of-plane and in-plane cases, the barrier height decreased upon increasing the number of CdSe nanorods.

Keywords:

[1] a) T. Ruotsalainen, J. Turku, P. Heikkilä, J. Roukolainen, A. Nykänen, T. Laitinen, M. Torkkeli, R. Serimaa, G. T. Brinke, A. Harlin, O. Ikkala, *Adv. Mater.* **2005**, *17*, 1048–1052; b) S. Valkama, H. Kosonen, J. Ruokolainen, T. Haatainen, M. Torkkeli, R. Serimaa, G. T. Brinke, O. Ikkala, *Nat. Mater.* **2004**, *3*, 872–876.

[2] a) M. Park, C. Harrison, P. M. Chaikin, R. A. Register, D. H. Adamson, *Science* **1997**, *276*, 1401–1404; b) Y. L. Loo, R. A. Register, A. J. Ryan, *Macromolecules* **2002**, *35*, 2365–2374.

[3] a) M. J. Misner, H. Skaff, T. Emrick, T. P. Russell, *Adv. Mater.* **2003**, *15*, 221–224; b) D. H. Kim, S. H. Kim, K. Lavery, T. P. Russell, *Nano Lett.* **2004**, *4*, 1841–1844; c) Y. Lin, A. Böker, J. He, K. Sill, H. Xiang, C. Abetz, X. Li, J. Wang, T. Emrick, S. Long, Q. Wang, A. Balazs, T. P. Russell, *Nature* **2005**, *434*, 55–59.

[4] a) A. M. Urbas, M. Maldovan, P. DeRege, E. L. Thomas, *Adv. Mater.* **2002**, *14*, 1850–1853; b) M. Bockstaller, R. Olb, E. L. Thomas, *Adv. Mater.* **2001**, *13*, 1783–1786.

[5] a) J. P. Spatz, S. Mossmer, C. Hartmann, M. Möller, T. Herzog, M. Krieger, H. G. Boyen, P. Ziemann, B. Kabius, *Langmuir* **2000**, *16*, 407–415; b) J. P. Spatz, V. Z.-H. Chan, S. Mößmer, F.-M. Kamm, A. Plettl, P. Ziemann, M. Möller, *Adv. Mater.* **2002**, *14*, 1827–1832.

[6] a) S. W. Yeh, K. H. Wei, Y. S. Sun, U. S. Jeng, K. S. Liang, *Macromolecules* **2003**, *36*, 7903–7907; b) C. C. Weng, K. H. Wei, *Chem. Mater.* **2003**, *15*, 2936–2941; c) C. C. Weng, K. F. Hsu, K. H. Wei, *Chem. Mater.* **2004**, *16*, 4080–4086; d) C. C. Weng, C. P. Chen, C. H. Ting, K. H. Wei, *Chem. Mater.* **2005**, *17*, 3328–3330; e) S. W. Yeh, K. H. Wei, Y. S. Sun, U. S. Jeng, K. S. Liang, *Macromolecules* **2005**, *38*, 6559–6565; f) S. W. Yeh, Y. T. Chang, C. H. Chou, K. H. Wei, *Macromol. Rapid Commun.* **2004**, *25*, 1680–1686.

[7] a) X. Duan, Y. Huang, R. Agarwal, C. M. Lieber, *Nature* **2003**, *421*, 241–245; b) Y. Cui, Q. Wei, H. Park, C. M. Lieber, *Science* **2001**, *293*, 1289–1292.

[8] L. K. van Vugt, S. J. Veen, E. P. A. M. Bakkers, A. L. Roest, D. Vanmaekelbergh, *J. Am. Chem. Soc.* **2005**, *127*, 12357–12362.

[9] M. Artemyev, B. Möller, U. Woggon, *Nano Lett.* **2003**, *3*, 509–512.

[10] F. Kim, S. Kwan, J. Akana, P. Yang, *J. Am. Chem. Soc.* **2001**, *123*, 4360–4361.

[11] a) W. U. Huynh, J. J. Dittmer, A. P. Alivisatos, *Science* **2002**, *295*, 2425–2427; b) J. Hu, L. S. Li, W. Yang, L. Manna, L. W. Wang, A. P. Alivisatos, *Science* **2001**, *292*, 2060–2063; c) L. S. Li, A. P. Alivisatos, *Adv. Mater.* **2003**, *15*, 408–411.

[12] Y. W. Su, C. S. Wu, C. C. Chen, C. D. Chen, *Adv. Mater.* **2003**, *15*, 49–51.

[13] M. H. Huang, S. Mao, H. Feick, H. Yan, Y. Wu, H. Kind, E. Weber, R. Russo, P. Yang, *Science* **2001**, *292*, 1897–1899.

[14] a) O. Harnack, C. Pacholski, H. Weller, A. Yasuda, J. M. Wessels, *Nano Lett.* **2003**, *3*, 1097–1101; b) P. A. Smith, C. D. Nordquist, T. N. Jackson, T. S. Mayer, B. R. Martin, J. Mbindyo, T. E. Mallouk, *Appl. Phys. Lett.* **2000**, *77*, 1399–1401.

[15] R. A. Mrozek, T. A. Taton, *Chem. Mater.* **2005**, *17*, 3384–3388.

[16] a) T. Xu, A. V. Zvelindovsky, G. J. A. Sevink, O. Gang, B. Ocko, Y. Zhu, S. P. Gido, T. P. Russell, *Macromolecules* **2004**, *37*, 6980–6984; b) H. Xiang, Y. Lin, T. P. Russell, *Macromolecules* **2004**, *37*, 5358–5363.

[17] H. A. Pohl, *J. Appl. Phys.* **1951**, *22*, 869–871.

[18] L. S. Li, A. P. Alivisatos, *Phys. Rev. Lett.* **2003**, *90*, 097402.

[19] a) D. Xu, G. D. Watt, J. N. Harb, R. C. Davis, *Nano Lett.* **2005**, *5*, 571–577; b) Y. Kawabe, M. M. Morrell, G. E. Jabbour, S. E. Shahen, B. Kippelen, *J. Appl. Phys.* **1998**, *84*, 5306–5314.

[20] P. W. M. Blom, M. J. M. de Jong, J. J. M. Vleggar, *Appl. Phys. Lett.* **1996**, *68*, 3308–3310.

[21] Z. A. Peng, X. Peng, *J. Am. Chem. Soc.* **2002**, *124*, 3343–3353.